Cell morphology and migration linked to substrate rigidity

Yong Ni and Martin Y. M. Chiang†*

Received 6th March 2007, Accepted 5th July 2007
First published as an Advance Article on the web 25th July 2007
DOI: 10.1039/b703376a

A mathematical model, based on thermodynamics, was developed to demonstrate how substrate rigidity influences cell morphology and migration. The mechanisms by which substrate rigidity are translated into cell-morphological changes and cell movement are described. The model takes into account the competition between the elastic energies in the cell–substrate system and work of adhesion at the cell periphery. The cell morphology and migration are dictated by the minimum of the total free energy of the cell–substrate system. By using this model, reported experimental observations on cell morphological changes and migration can be better understood with a theoretical basis. In addition, these observations can be more accurately correlated with the variation of substrate rigidity. This study indicates that the activity of the adherent cell is dependent not only on the substrate rigidity but also is correlated with the relative rigidity between the cell and substrate. Moreover, the study suggests that the cell stiffness can be estimated based on the substrate stiffness corresponding to the change of trend in morphological stability.

1. Introduction

Cell adhering to a flat deformable substrate can sense the mechanical stimuli,[1–6] respond to changes in the balance of cellular forces (intra- and extracellular forces),[7,8] and regulate many important physiological processes.[9–16] Previous *in vitro* studies using cells cultured on substrates have shown that cell activity is influenced by substrate mechanics in the following ways. 1) Cells are able to sense the variation in substrate rigidity since certain types of cells on stiffer substrates have less rounded morphologies, and are more likely to extend into branched morphologies than the same cells on softer substrates.[17–19] In contrast, some experimental studies show that other cell types extend into more branches on softer substrates, and exhibit no preference to branching on stiffer ones.[20–22] 2) It has also been observed that when cells are cultured on a cyclically stretched substrate, the cells tend to elongate perpendicularly to the direction of stretch.[23–26] 3) Experiments have shown that cells prefer to migrate towards stiffer regions on a substrate with a stiffness gradient, which is known as durotaxis.[27–30] A number of models based on thermodynamics have recently appeared in the literature as an attempt to elucidate the complexities of effects due to mechanical interactions between the cell and substrate on cellular organization,[31–34] cell adhesion[25,35–45] and migration.[46–49] However, how exactly the substrate rigidity influences the cell morphology and migration, and how the mechanisms by which substrate rigidity are translated into cell-morphological changes and cell movement, still remain elusive. Our objective is to formulate a mathematical model and analysis that will provide insight into the dependency of cell morphology and migration on substrate rigidity. This insight cannot be deduced from the experimental observations alone.

In vitro studies using cells adherent to various flexible substrates have detected and quantified cellular tractions associated with the focal adhesion (FA), a molecular complex known as a mechanosensor, which is formed at the site of the cell adhesion to the substrate (*i.e.*, cell periphery).[50,51] Through the FAs, cells sense physicochemical signals that mutually transmit between the cell and substrate, and the tractions balance the mechanical forces generated internally through the intracellular contractile machinery, or applied externally through the extracellular matrix.[52,53] As a result, cells can guide mechanosensitive cellular activities, such as morphological changes, stability and migration, and the development of FAs even if the surrounding chemical signals are identical (see recent reviews[2-6]). More importantly, these mechanosensitive activities, which in turn are mediated by the tractions, can convert mechanical signals (forces) into changes in cellular biochemistry to direct the cell growth and development.

Guided by the aforementioned experimental observations, we have developed a mathematical model of cell–substrate adhesion, which effectively reflects the mechanical changes in the extracellular environment, to explain the dependency of cell morphology and migration on substrate rigidity. The hypothesis in the model is that the morphology of a cell adhering to a substrate is characterized by the competition between strain energies (in the cell and substrate) and interfacial energy (work of adhesion at the cell periphery), and that the final configuration (or stability) of the cell morphology is determined by the minimum of the total free energy of the cell–substrate system. Thus, the cell changes into its energetically favorable shape by the assembling/disassembling of focal adhesions distributed around the cell periphery. The phase-field method, which provides a mathematical description to free-boundary problems for phase transitions,[54] is adapted to simulate cell migration associated with evolving cell morphology due to the variation of substrate

Polymers Division, National Institute of Standards and Technology (NIST), Gaithersburg, MD, 20899, USA.
E-mail: martin.chiang@nist.gov
† To whom all correspondence should be addressed (martin.chiang@nist.gov).

rigidity. Our analyses on the morphological changes and migrations are consistent with experimental observations reported in the literature for various types of cell–substrate systems. This agreement is a necessary condition towards validating the hypothesis, for the morphological stability of the cell used in the study. More importantly, the study suggests that the cell stiffness can be estimated based on the substrate stiffness corresponding to the change in trend in morphological stability. In the next section, the fundamental equations derived for the relationship of the total free energies with the substrate rigidity will be presented. Results and discussion on the morphological stability of cells due to isotropic and anisotropic substrate mechanics, and on the migrations of cells due to gradient-substrate rigidity will be given in subsequent sections.

2. Fundamental basis for the total free energy in a cell–substrate system

In this study, a cell is assumed to be a two-dimensional flat elastic membrane, while the substrate is assumed to be a three-dimensional elastic structure. Our model is based on minimizing the total free energy of cell–substrate system. We express the total free energy, E_{tot}, as a sum of strain-energy component, E_1, and interfacial energy component, E_2. It is assumed that the focal adhesions are already established between the cell and substrate. Each focal adhesion, generating a traction along the stress fiber of cell, is modeled as a point loading exerting on the substrate surface at the cell periphery (surface traction Fig. 1) since FAs tend to form toward the cell periphery.[36,50] For mathematical simplicity, these tractions are modeled as 1) shear stress continuously distributed along the cell periphery, and 2) normal to the cell periphery in accordance to experimental observations.[56–59] If neglecting details of the active response of the cell to the mechanical stimuli, one can assume that the cell–substrate system is in a state of mechanical equilibrium, such that the tractions are always balanced between the intercellular and extracellular forces. Due to this mechanical coupling between the cell and substrate, the change of substrate rigidity will inevitably mediate the cell morphology and migration through the assembling/disassembling process of FAs. Mathematically, the tractions,τ_α, can be expressed as follows:

$$\tau_\alpha = \sigma^{c}_{\alpha\beta}\delta(\boldsymbol{x} - r\boldsymbol{e}_r)n_\beta(l), \text{ and } \tau_\alpha = \sigma^{s}_{\alpha 3}, \quad (1)$$

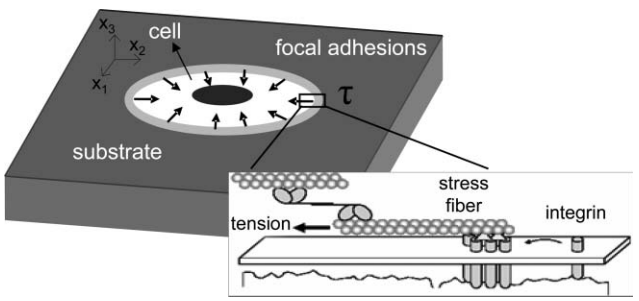

Fig. 1 Schematic of an adherent cell on elastic substrate with focal adhesions concentrating at the cell periphery. Tractions are generated along stress fibers through myosin contraction and transmitted into the substrate across integrin linkages.[55]

where $\sigma_{\alpha\beta}$ and $\sigma_{\alpha 3}$ are the components of the stress tensor. The superscripts c and s represents cell (intracellular) and substrate (extracellular), respectively; $\delta(x)$ is the Dirac's source function; $\boldsymbol{x} = (x_1,x_2)$; $r\boldsymbol{e}_r$ is the vector of the cell periphery in the polar coordinate system with $\boldsymbol{e}_r$ the base vector of r axis; n_β, the component of the inward normal vector to the cell periphery, is a function of circumferential path, l. Throughout this manuscript, Greek subscripts of tensor index range from 1 to 2, while Latin subscripts run from 1 to 3. The usual summation convention is adopted for repeated indices in the tensor notation. It is known, from eqn (1), that the tractions are fully coupled with the elasticity of the cytoskeleton and substrate; therefore, instead of a closed-form solution, numerical methods for the solution of eqn (1) have to be pursued.

The intracellular stress balanced by the tractions is reported to increase with the increase of substrate rigidity, and it has a maximum due to the limit of biochemistry.[43,44,60–64] Accordingly, for simplicity, a two-serial spring model[65] has been adapted in our study to describe the mechanical coupling at the position of each focal adhesion. The substrate and the intracellular structure are represented by harmonic springs with spring constants μ^s and μ^c, which correspond to the local isotropic shear moduli of the cell and substrate, respectively. The intracellular stress $\sigma^{c}_{\alpha\beta}$ can then be analytically expressed as:

$$\sigma^{c}_{\alpha\beta} = \frac{\sigma^{0}_{\alpha\beta}}{(1+\mu^c/\mu^s)}, \quad (2)$$

where $\sigma^{0}_{\alpha\beta}$ are the components of saturated intracellular stress tensor in the cell, and can be estimated by measuring the traction *via* various traction force microscopy[56–59] (this corresponds to the limiting case when the substrate is rigid). It is worthwhile to note that $\sigma^{0}_{\alpha\beta}$, μ^c and μ^s may be non-uniform if there are significant heterogeneities. From eqn (1) and (2), the expression for the traction can be obtained as:

$$\tau_\alpha = \frac{\sigma^{0}_{\alpha\beta}\delta(\boldsymbol{x}-r\boldsymbol{e}_r)n_\beta(l)}{(1+\mu^c/\mu^s)} \quad (3)$$

Eqn (3) describes how the substrate rigidity influences the traction. The result from this equation is consistent with that obtained from the models recently reported in the literature,[43,44,63] in which some key biochemical processes that actively regulate the tractions are taken into consideration.

The displacement of a point $\boldsymbol{x}$ on the substrate surface, u^s_α, induced by the traction forces, can be obtained as:

$$u^s_\alpha(\boldsymbol{x}) = \int_A G_{\alpha\beta}(\boldsymbol{x},\boldsymbol{x}')\tau_\beta(\boldsymbol{x}')\mathrm{d}\boldsymbol{x}', \quad (4)$$

where $\boldsymbol{x} = (x_1,x_2)$, and $\boldsymbol{x}'$ is a dummy variable. $G_{\alpha\beta}(\boldsymbol{x},\boldsymbol{x}')$ are the components of surface Green's function tensor for an isotropic elasticity

$$G_{\alpha\beta}(\boldsymbol{x},\boldsymbol{x}') = \frac{1}{2\pi\mu^s}\left[\frac{(1-\nu^s)\delta_{\alpha\beta}}{|\boldsymbol{x}-\boldsymbol{x}'|} + \frac{\nu^s(\boldsymbol{x}-\boldsymbol{x}')_\alpha(\boldsymbol{x}-\boldsymbol{x}')_\beta}{|\boldsymbol{x}-\boldsymbol{x}'|^3}\right], \quad (5)$$

where ν^s is the Poisson's ratio of the substrate, and δ_{ij} is the Kronecker delta tensor. The free energy contributed by the

elastic responses in the substrate and cell, E_1, can then be effectively expressed as follows:

$$E_1 = \frac{1}{2}\int_V \sigma_{ij}\,\varepsilon_{ij}\,\mathrm{d}V - \int_A \tau_\alpha\, u_\alpha^s\,\mathrm{d}A, \tag{6}$$

where σ_{ij} and ε_{ij} are the components of stress and strain tensors, respectively. u_α^s is the displacement of the substrate. V is the volume of the substrate, and A the surface area of the substrate. For a linear elastic system one can have:

$$\frac{1}{2}\int_V \sigma_{ij}\,\varepsilon_{ij}\,\mathrm{d}V = \frac{1}{2}\int_A \tau_\alpha\, u_\alpha^s\,\mathrm{d}A \tag{7}$$

Thus, E_1 becomes:

$$E_1 = -\frac{1}{2}\int_A \tau_\alpha\, u_\alpha^s\,\mathrm{d}A \tag{8}$$

Another free energy in the cell–substrate system is the interfacial energy, E_2 (work of adhesion), stored in a narrow strip along the edge of the cell at the focal adhesions. E_2 is the energy cost during the protein aggregation of FA, such as the contribution of translational entropy, and biochemical reaction energy.[66,67] In this study, it is assumed that a homogenous interfacial energy density (γ, per unit length) exists, and is uniformly distributed along the cell edge. Thus,

$$E_2 = \int_L \gamma\,\mathrm{d}l, \tag{9}$$

where L is the total peripheral length of the cell, which varies during the change of cell morphology, although it is assumed that the volume of the cell is conserved and the cell thickness remains constant. Finally, the total free energy, E_{tot}, is expressed as:

$$E_{tot} = E_1 + E_2, \tag{10}$$

and the final configuration (or stability) of the cell morphology is determined according to the minimum of this total free energy.

3. Morphological stability of cell due to isotropic traction

To understand the morphological stability of the adherent cell, the cell with an initial circular configuration is assumed to have an isotropic traction (isotropic pre-stress, *i.e.*, $\sigma_{\alpha\beta}^0 = \sigma_0\delta_{\alpha\beta}$, where σ_0 is a constant) and experiences a small morphological perturbation of the harmonic form at its edge, Fig. 2. This perturbation can be described mathematically as:

$$r(\theta) = R_0 + \sum_n \delta_n \exp(in\theta) \tag{11}$$

where R_0 and r are the radii of the cell at the initial state and perturbed state, respectively. n is a positive integer, denoting the discrete azimuthal wave number, i is the imaginary unit and δ_n represents the perturbation amplitude of the nth mode. By adapting a similar solution method used for lipid monolayer systems,[68] the variation of total free energy

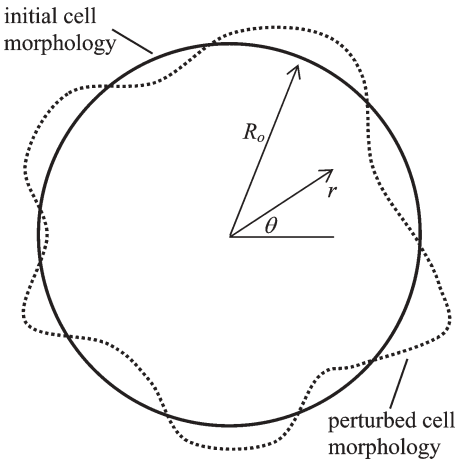

Fig. 2 An initially circular cell (solid line) undergoing a morphological perturbation of harmonic form (dotted line).

associated with this edge perturbation, ΔE_{tot}, can be obtained up to a quadratic order as:

$$\Delta E_{tot} = \frac{2\pi}{R_0}\sum_n \omega_n\,|\delta_n|^2, \tag{12}$$

with the normalized ω_n being:

$$\frac{2\pi\mu^s\omega_n(1+\mu^c/\mu^s)^2}{\sigma_0^2(1-\nu^s)} = 2\pi\beta\left(n^2-1\right) - 2[B_1 - B_n], \tag{13}$$

where β, the ratio of interfacial energy density to strain energy density of the cell–substrate system, is defined as:

$$\beta = \mu^s\gamma(1 + \mu^c/\mu^s)^2/(1 - \nu^s)\sigma_0^2, \tag{14}$$

with μ^s and ν^s being the shear modulus and the Poisson ratio of the substrate, respectively. The B_n is given as:

$$B_n = -\frac{Q_{n-1/2}^1\left(1+a_0^2/2R_0^2\right)}{(a_0/R_0)\left(1+a_0^2/4R_0^2\right)^{1/2}}, \tag{15}$$

with $Q_{n-1/2}^1(x)$ being the associated Legendre function of the second kind. a_0 is a microscopic cut-off length that is taken to be the typical distance between two adjacent traction forces.

Mathematically, the stability of cell morphology is assessed by the sign associated with ω_n in eqn (13). In other words, if all the values of ω_1, ω_2, … and ω_n are positive, the cell is morphologically stable; otherwise, it is unstable against the subject edge perturbation. Physically, the stability of cell morphology is characterized by the competition between the interfacial energy (stabilizing the cell morphology) and the strain energies (destabilizing the cell morphology). More importantly, one can note that the normalized ω_n in eqn (13) dominates the variation of the total free energy of the cell–substrate system, and the parameter β takes the substrate rigidity into account through eqn (14). The relationship between ω_n and β plays an important role on the stability of cell morphology.

In our physical model, a cell would select an appropriate shape not by deforming, but by the competition between

adhesion and strain energies in the cell, such that the cell changes into its energetically favorable shape by the assembling/disassembling of focal adhesions distributed around the cell edge. To be clear, we considered an adherent cell with initial radius $R_0 = 20a_0$ subjected to a single-wave perturbation as:

$$r(\theta) = R_0 + \delta_n \exp(in\theta) \quad (16)$$

Fig. 3 shows the relationship between the variation of total free energy (ω_n) and the perturbation mode (n) for various substrate rigidities. The variation of the rigidity is reflected by the value of β, and a more detailed discussion on its role to the morphological change of cell will be given later in the manuscript. From the result in the figure, one can see that when β is large (*e.g.*, $\beta = 0.5$), ω_n is always positive and attains a minimum at $n = 1$. This indicates that any edge perturbation is *energetically unfavorable*, thus, the morphology of the cell is stable and remains in the initial circular configuration. With decreasing β, the ω_n–n curve minimum shifts more downwards, and the variation of total free energy can be negative. For example, when $\beta = 0.2$, ω_n is negative for most of the perturbation modes considered in the study. In such a case, the initial morphology of the cell becomes unstable for these perturbation modes, and $n \approx 8$ is the most energetically favorable perturbation mode. Fig. 3 indicates how the decrease of β gives rise to morphological instabilities (more branches). It should be noted here that these morphological predictions presented in Fig. 3 (insets) are not exactly what the experimental results should look like, since in a real case the morphology of active cells has been blurred by thermal fluctuation and non-equilibrium processes. However, the result in Fig. 3 is to demonstrate the dependency of cell morphology (branching) on the relative rigidity between the cell and substrate.

While the value of β is an index for the morphological stability of the cell, β shown in Fig. 3 does not explicitly reflect

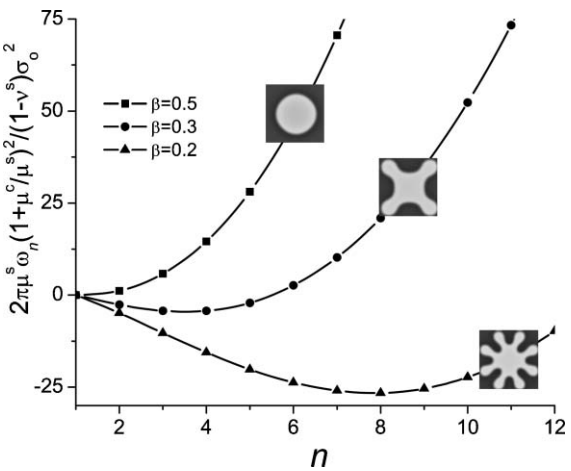

Fig. 3 The energy variation (expressed by $2\pi\mu^s\omega_n(1 + \mu^c/\mu^s)^2/(1 - \nu^s)\sigma_0^2$) as a function of perturbation mode n for different values of β due to changes of the substrate rigidity. The insets are the corresponding final stable configurations of the cell obtained from the phase-field simulation with the feature of nonlinearity (discussed later in the article).

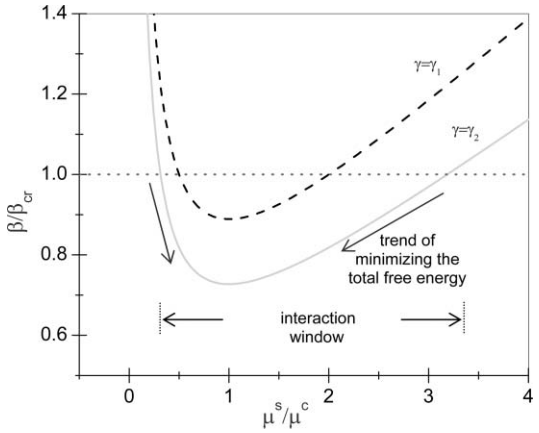

Fig. 4 The variation of β as a function of rigidity ratio, μ^s/μ^c, for various interfacial energies, γ_1 and γ_2 ($\gamma_1 > \gamma_2$), corresponding to different cell–substrate systems.

how the substrate rigidity changes (softer or harder) relative to the adherent cell. Fig. 4 gives the variation of β as a function of the stiffness ratio of the substrate to cell (μ^s/μ^c) *versus* interfacial energy, γ. The β is now normalized by a critical value, β_{cr}, which is determined by setting $\Delta E_{tot} \equiv 0$ and represents a characteristic value for a given initial cell morphology and perturbation mode of a cell–substrate system. When $\beta \geqslant \beta_{cr}$, the interfacial energy between the cell and substrate dominates the variation of total free energy; thus, the morphology of the cell is stable. For $\beta < \beta_{cr}$, the strain energy of the cell–substrate system dominates and the morphology becomes unstable. Fig. 4 is of particular interest when the substrate rigidity is comparable to that of the cell, because there is a window of the stiffness ratio (μ^s/μ^c) in which β reaches its minimum and $\beta < \beta_{cr}$. Accordingly, one can argue that the morphological change of cell, due to the variation of substrate rigidity, only happens once the cell and substrate stiffness are comparable, such that a *sensible* interaction between the cell and substrate can take place (a maximum mechanical interaction energy between the cell and substrate). This argument can be supported by several related experimental observations reported in the literature, in which cells indeed show a morphological transition when the stiffness of their surrounding environment is similar to that of themselves,[17,18] and cells require an optimal substrate rigidity for normal function and differentiation.[10–16] From Fig. 4, one also can notice that the extent of this interaction (*i.e.*, the size of the window) is narrowed and up-shifted with the increase of interfacial energy between the cell and substrate. More importantly, Fig. 4 indicates that the change of trend in morphological stability (the inflection point) corresponds to $\mu^s/\mu^c = 1$. Therefore, the cell stiffness can be estimated by observing this change, Fig. 5.

In experimental observations, for fibroblast and endothelial cells with shear moduli on the order of $\approx$ 4000 Pa, their morphological transition occurs at substrates with shear moduli from 1000 to 3000 Pa, and they prefer to extend into more branches on stiffer substrates.[17,18] Fibroblasts show no preference in branching on substrates with low stiffness (50 to 550 Pa). These observations can be notably explained using the

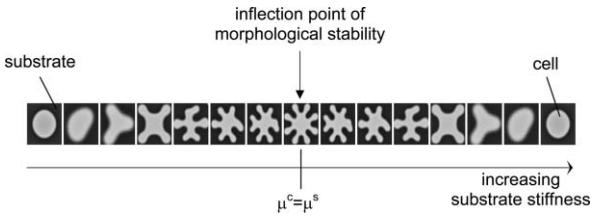

Fig. 5 Schematic representing how cell morphology changes in response to substrate rigidity. At the inflection point (the change of trend in morphological stability), the cell rigidity is identical substrate rigidity. This fact can be used to estimate cell rigidity.

qualitative result in Fig. 4, in which when the cell stiffness is comparable with and *larger* than the substrate stiffness (*i.e.*, $\mu^s/\mu^c \leqslant 1$, the left-hand side of the window in Fig. 4), the cell morphology becomes more unstable (more occurrence of morphological transition) with *increasing* the substrate rigidity. Also, the result described in Fig. 4 indicates that cell morphology becomes stable when a cell has much higher stiffness than the substrate (*i.e.*, this is equivalent to the experiment with fibroblasts on substrates with very low stiffness; *i.e.*, 50 to 550 Pa).

Contrasting to fibroblasts, the experimental study of neuronal processes, on substrates with shear moduli ranging from 50 to 550 Pa, shows that nerve cells extend into more branches on softer substrates and no preference in branching on stiffer ones.[20–22] Unfortunately, in the study the stiffness of these nerve cells is not measured, only the shear modulus of bovine spinal cord is given as $\approx$ 50 Pa.[21] However, from our aforementioned mathematical model and experimental observations in the literature, it can be inferred that the modulus of nerve cell is in the region of 50 Pa. This inference can be rationalized using the results in Fig. 4, in which when the cell stiffness is comparable and *smaller* than the substrate stiffness (*i.e.*, $\mu^s/\mu^c \geqslant 1$, the right-hand side of the window in Fig. 4), the cell morphology becomes more unstable with *decreasing* substrate rigidity (softer).

4. Morphological stability of cell due to anisotropic traction

Experimental observations have shown that, when cells are cultured on a cyclically stretched substrate, the cells can reorient themselves in a manner associated with their stress fibers and adopt anisotropic morphologies.[23–26] Here, we assumed that the driving force for the formation of anisotropy is due to the anisotropic traction developed at the cell-adhesion sites. In this study, to formulate a model describing the morphological stability due to the anisotropic tractions, the underlying substrate of an adherent cell exerts a biaxial stretching that results in anisotropic tractions, τ_1 and τ_2, distributed along the cell periphery (see the inset of Fig. 5), where $\tau_1 = \sigma^o_{11}\delta(\boldsymbol{x} - r\boldsymbol{e}_r)/(1 + \mu^c/\mu^s)$ and $\tau_2 = \sigma^o_{22}\delta(\boldsymbol{x} - r\boldsymbol{e}_r)/(1 + \mu^c/\mu^s)$ are tractions in the x_1 and x_2 directions, respectively (based on eqn 3). In the model, the anisotropy of the traction is characterized by a parameter η, defined as $\eta = \tau_1/\tau_2$. The cell size, D, remains constant and is defined as $D = \sqrt{ab}$, where a and b are the principal axes of the cell in the x_1 and x_2 directions,

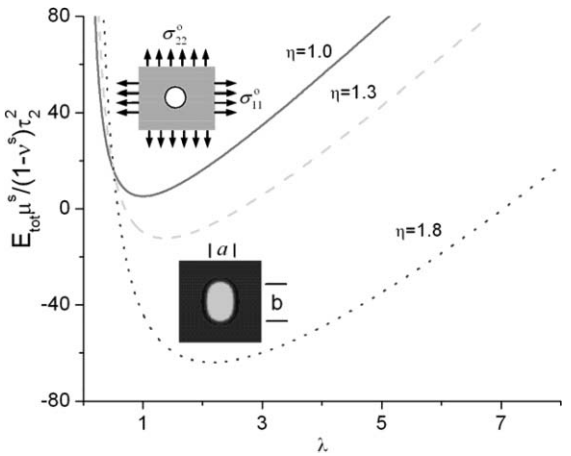

Fig. 6 The energy variation ($E_{tot}\mu^s/(1 - \nu^s)\tau_2^2$) *vs.* the degree of morphological anisotropy ($\lambda = a/b$) for a given cell–substrate system under various traction ratios ($\eta = \tau_1/\tau_2$). The inserts are the corresponding configurations of the cell obtained from the phase-field simulation (discussed later in the manuscript).

respectively. The cell shape is assumed to be round prior to the stretching, *i.e.*, $a = b$; if $a \neq b$ during the stretching, then, the cell shape will be elliptic. Thus, for a given size of cell subjected to anisotropic tractions, the cell shape is optimized by varying a and b under the constraints of constant D and the minimal total free energy of the cell–substrate system. Also, the degree of morphological anisotropy of the cell (*i.e.*, the anisotropic elongation of cell) is characterized by a parameter, λ, defined as $\lambda = b/a$.

Fig. 6 gives the result of energy variation as a function of λ for different degrees of anisotropy in traction force, η. The result is based on $D = 15a_0$, and $\beta = 0.3$ ($\beta = \mu^s\gamma/(1 - \nu^s)\tau_2^2$). When $\eta = 1$, the cell is subjected to isotropic tractions, the result in Fig. 6 indicates that the energy variation has a minimum at $\lambda = 1$, which corresponds to $a = b$. This implies that the cell does not have any specific preference for the direction of elongation and, consequently, adopts a round morphology. For the case of $\eta > 1$, the minimum of energy variation shifts away from $\lambda = 1$ and towards a larger value of λ ($a < b$). This suggests that the cell tends to elongate perpendicular (see the inset of Fig. 6) to the direction of larger traction, which is in the x_1 direction in this case since $\eta > 1$. The result of our theoretical analysis, in Fig. 6, on the morphological anisotropy of cell, is consistent with related experimental observations[23,24] and other theoretical predictions based on a principle of minimum strain energy[25] or contact mechanical models[37,38] reported in the literature. In these observations, the direction of stretch applied to the substrate is in line with the direction of larger traction in the cell, however, the cell elongates to a direction perpendicular to the direction of stretch.

Interestingly, in a different experimental study,[26] it was found that cells and their stress fibers oriented parallel (instead of perpendicular found in ref. 23, 24) to the direction of uniaxial stretch applied to the substrate. It was discovered that this parallelism is due to blocking of the Rho activity in the cell during the stretch. Biologically, this activity sends chemical signals to enhance the nucleation of stress fibers with focal adhesions (FAs) localized at their ends.[26] Thus, the

reorganization and perpendicular orientation of stress fibers in response to uniaxial strain is a consequence of Rho activity. As mentioned earlier, in our model the assembly/disassembly of FAs, which gives the redistribution of traction forces, occurs at the cell periphery during the morphological changes of the cell. Therefore, in a sense, our model is effectively equivalent to allowing Rho activity for regulating FA dynamics by nucleation of stress fibers. Also, our prediction on cell orientation is consistent with that reported in the literature,[41,42] in which the cell orientation was considered as a stability problem on the basis of nonlinear elasticity. The study in the literature has also concluded that zero/low prestress (intracellular stress) would lead the cells to align in the direction of largest substrate strain, whereas finite prestress would lead the cells to align away from the direction of largest substrate strain. Indeed, experimental observations have indicated that the prestress increases with the increase of Rho activity. From eqn (1), in our study, one can see that a larger prestress corresponds to a larger traction. Therefore, we expected the predictions from our model to agree with the model reported in the literature.[41,42]

5. Effect of substrate with stiffness gradient on the cell migration

In the previous two sections of the paper, effects of substrate rigidity and loading anisotropy (which also effectively speculates on the anisotropy of substrate rigidity) on the morphological changes of the cell have been discussed. In this section, a theoretical model is formulated to focus on cell locomotion due to the stiffness variation of a substrate to which the cell adheres. It is found that, when cells adhere to a substrate with a stiffness gradient, changes in the local stiffness of the substrate regulate not only the cell morphology and orientation but also the cell motility, such that the cell migrates from the softer region towards to the stiffer region of the substrate. This is known as durotaxis.[27–30] In this study, the cell migration due to the existence of the stiffness variation is hypothesized to be driven by the progressive minimization process of the total free energy in the cell–substrate system. To couple the cell migration with evolving cell morphology and orientation, the phase-field theory[54] is adapted to simulate the cell activity. In the theory, the phase-field variable $\phi(x_1,x_2,t)$ is introduced to denote the morphological profile of cell–substrate system such that $\phi = 1$ stands for the adherent cell phase, while $\phi = 0$ for the exposed substrate phase. The cell periphery is represented by a thin continuous transition region where the value of ϕ sharply changes between 0 and 1. Since the system is mass conservative, $\phi(x_1,x_2,t)$ satisfies the Cahn–Hilliard equation[54] as follows:

$$\frac{\partial\phi}{\partial t} = \nabla\left(\frac{D(\phi)}{\Lambda k_B T}\nabla\frac{\delta E_{tot}}{\delta\phi}\right), \tag{17}$$

in which ∇ is the two-dimensional gradient operator. Λ is the number of FAs per unit area on the substrate surface, k_B Boltzmann's constant, and T the absolute temperature. $D(\phi) = D_0\phi^2(1-\phi)^2$ reflects the mobility of cell that is driven by the dynamics of focal adhesion assembly/disassembly. This motility occurs mainly at the cell periphery, where D_0 is a constant. E_{tot}, the ϕ-dependent total free energy of the cell–substrate system, is expressed as:

$$E_{tot}(\phi) = \int_A \left(g(\phi) + \varepsilon_\phi \phi_{,a}\phi_{,a}\right)dx_1dx_2 + \frac{1-v^s}{4\pi\mu^s}\int_A\int_A \frac{f(\phi(\mathbf{x}))f(\phi(\mathbf{x}'))d\mathbf{x}d\mathbf{x}'}{\left((x_1-x_1')^2+(x_2-x_2')^2\right)^{3/2}}, \tag{18}$$

with the first term $g(\phi)$ representing the pure chemical potential. In this study, a double-well function of $g(\phi) = g_0\phi^2(1-\phi)^2$ is used, where g_0 is a positive constant. This function has two minima corresponding to the exposed substrate phase and the adherent cell phase, respectively. The second term of eqn 18 is the Cahn–Hilliard gradient energy[54] accounting for the interfacial energy, where ε_ϕ is the coefficient of gradient energy. The last term represents the elastic energies in the cell and substrate with $f(\phi) = \sigma_0/(1+\mu^c/\mu^s)\phi$. The hydrostatic strain on the substrate surface induced by the tractions, $u^s_{a,a}$, can be expressed using the Green function technique as:

$$u^s_{a,a} = \frac{1-v^s}{2\pi\mu^s}\int_A \frac{f(\phi(\mathbf{x}'))d\mathbf{x}'}{\left((x_1-x_1')^2+(x_2-x_2')^2\right)^{3/2}}, \tag{19}$$

and the strain energy in eqn (18) can be rewritten as:

$$\frac{1-v^s}{4\pi\mu^s}\int_A\int_A \frac{f(\phi(\mathbf{x}))f(\phi(\mathbf{x}'))d\mathbf{x}d\mathbf{x}'}{\left((x_1-x_1')^2+(x_2-x_2')^2\right)^{3/2}} = \frac{1}{2}\int_A f(\phi(\mathbf{x}))u^s_{a,a}(\mathbf{x})d\mathbf{x} \tag{20}$$

Noting that $\tau_a = \partial f(\phi(\mathbf{x}))/\partial x_a$ and applying the Gauss theorem to eqn (20), it is apparent that the expression of the strain energy in eqn (18) is consistent with that in eqn (8).

In this study, a semi-implicit Fourier-spectrum method was carried out for eqn (17),[69] in a representative subdivision of the substrate having a size of $128l_0 \times 128l_0$. $l_0 = \sqrt{\varepsilon_\phi/\Lambda k_B T}$ being a characteristic length. Also, a periodic boundary condition is imposed at the circumference of the subdivision. The map of substrate stiffness, which is reflected in the variation of β ($\beta = \mu^s\gamma(1+\mu^c/\mu^s)^2/(1-v^s)\sigma_0^2$, $\gamma = \sqrt{\varepsilon_\phi\Lambda k_B T/3}$), is given in Fig. 7a. Initially, the cell had a circular morphology with a radius $R_0 = 12l_0$ and adhered to the substrate surface having a lower stiffness. In such a case, the interfacial energy dominates the total free energy of the cell–substrate system and the cell should maintain a rounded morphology. Fig. 7b–7f show a typical evolution path of the cell from the initial stage to the final stage of the simulation. One can see that the cell migrates from the substrate surface with lower stiffness to higher stiffness. Also, it is interesting to note that when the cell migrates to a region on the substrate surface with a critical stiffness, the cell morphology becomes unstable and changes from the original shape to a "potato"-like shape, Fig. 7f. This phenomenon is attributed to a consequence of the competition between energies for the morphological change and the migration, since during the cell migration the substrate rigidity also mediates the cell morphology in order to

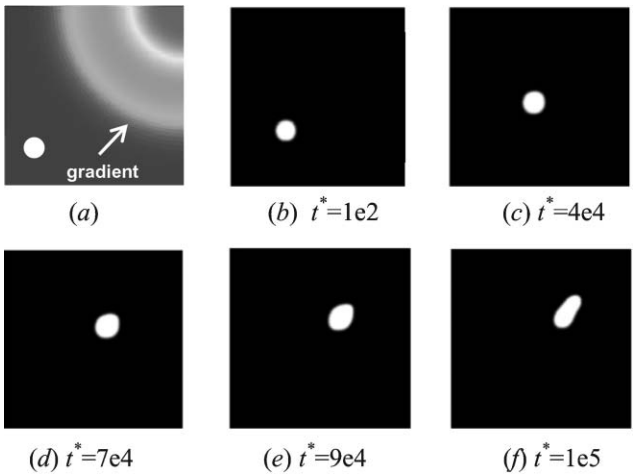

Fig. 7 A circular cell initially located on the softer region of substrate with a stiffness gradient represented by the map of β (a), where $\beta = 1/6(1 + 0.3e^{-[(x_1-128l_o)2+(x_2-128l_0)2]})$ and l_0 is a characteristic length; the simulated snapshots of cell migration towards to stiffer regions of substrate at different time frames (b)–(f), where $t^* = t/t_0$ with $t_0 = l_0^2/D_0$.

obtain a state possessing the minimal total free energy. Based on the results in the figure, one can suggest that the durotaxis reported in the literature[27–30] might be viewed as the process of minimizing the total free energy of the cell–substrate system.

Besides the simulation presented in Fig. 7, the durotaxi phenomenon can also be illustrated using the result shown in Fig. 4. Since the ratio of substrate to cell stiffness is assumed to be less than one ($\mu^s/\mu^c \leqslant 1$) in the simulation, notably from Fig. 4, the substrate stiffness must be increased in order to have a decreasing β such that the minimal total free energy in the cell–substrate system can be reached. In other words, in order to get an energetically favorable (or more stable) cell configuration on the substrate, the cell would migrate from a region of lower stiffness to a region of higher stiffness on the substrate. The result from Fig. 4 also predicts that the cell would migrate from the stiffer regions of the substrate towards to the softer regions if the substrate is stiffer than the cell ($\mu^s/\mu^c \geqslant 1$). However, to the best of our knowledge, no experimental observation of this "reverse" durotaxis is reported to support our argument. This may be due to the fact that our model does not incorporate the effect of substrate rigidity on the change of cell stiffness. In fact, many cells tend to actively increase their stiffness with increased substrate rigidity.[60–64]

6. Concluding remarks

In this study, we have developed mathematical models to describe a) how cell morphology is linked to substrate rigidity, b) how cell migration is guided by substrate rigidity, and c) the mechanisms by which substrate rigidity is translated into cell-morphological stability and movement. Consistent with experimental observations reported in the literature, our model has demonstrated that the morphological stability of an adherent cell to substrate is governed by the minimal total free energy in the cell–substrate system. The morphological changes of a cell can be rationalized as the consequence of competition between interfacial and elastic energies in the total free energy of cell–substrate system. The interfacial energy between the cell and substrate stabilizes the cell morphology while the strain energy from intracellular and extracellular forces destabilizes it. The competition results in a "resonant" window that refers to the range of the stiffness ratio (μ^s/μ^c, substrate to cell) over which the cell is in *interaction* with the substrate. With this interaction, the cell and substrate can be *mutually compliant*. In other words, in this *sensible interaction*, the mechanical interaction energy between the cell and substrate reaches a maximum. Consequently, it becomes energetically favorable for the cell to undergo significant morphological changes and for normal function and differentiation. The width of the window and the amplitude of the interaction response are influenced by the amount of interfacial energy, which is cell–substrate specific. More importantly, the results from our theoretical analysis suggest that the cell stiffness can be estimated based on the substrate stiffness corresponding to the change of trend in morphological stability. Additionally, by adapting the phase-field theory, our theoretical model has reasonably simulated the cell migration and orientation due to the variation of substrate stiffness and confirmed that the durotaxis can be viewed as a *progressive* minimization of the total free energy in a cell–substrate system.

In our model, the cell is assumed to be a 2D homogeneous elastic system, whereas in reality it is a 3D heterogeneous viscoelastic system. In addition, the model has not taken into account the non-linear, stiffening stress-strain behavior of the cells, and biochemical processes when cells adhere to a substrate. In fact, the resultant process of cell adhesion is even more complicated at cell molecular level (cytoskeletal proteins, contractile apparatus, *etc.*). For example, cell adhesions are adaptive on the molecular level and actively governed by the receptor–ligand bonds.[70,71] The nonlinear dynamics and various types of bonds are found to result in a bistability state of cell adhesions[72,73] (between bounded and unbounded states) and a size-dependent focal adhesion domain.[74] For these cases, instead of a homogenous adhesion energy density used in eqn (9), a statistical description of cell adhesion may be necessary. Also, the response of cells to external mechanical stimuli is actively regulated by some key biochemical processes,[43,44] such as i) an activation signal that triggers actin polymerization and myosin phosphorylation, ii) the tension-dependent assembly of actin and myosin into stress fibers, and iii) the cross-bridge cycling between actin and myosin filaments that generates the tensions, and balances the cellular traction forces. The effects of these more realistic cell behaviors should be considered in a future refined model. Finally, despite those simplifications made in this study, we believe that our approach captures the main features of the substrate rigidity effect on the cell–substrate system.

References

1 N. Wang, J. P. Butler and D. E. Ingber, *Science*, 1993, **260**, 1124–1127.
2 D. E. Discher, P. Janmey and Y. L. Wang, *Science*, 2005, **310**, 1139–1143.

3 P. C. Georges and P. A. Janmey, *J. Appl. Physiol.*, 2005, **98**, 1547–1553.
4 I. Levental, P. C. Georges and P. A. Janmey, *Soft Matter*, 2007, **3**, 299–306.
5 U. S. Schwarz, *Soft Matter*, 2007, **3**, 263–266.
6 V. Vogel and M. Sheetz, *Nat. Rev. Mol. Cell Biol.*, 2006, **7**, 265–275.
7 M. E. Chicurel, C. S. Chen and D. E. Ingber, *Curr. Opin. Cell Biol.*, 1998, **10**, 232–239.
8 C. G. Galbraith and M. P. Sheetz, *Curr. Opin. Cell Biol.*, 1998, **10**, 566–571.
9 C. S. Chen, M. Mrksich, S. Huang, G. M. Whitesides and D. E. Ingber, *Science*, 1997, **276**, 1425–1428.
10 A. J. Engler, M. A. Griffin, S. Sen, C. G. Bonnetnann, H. L. Sweeney and D. E. Discher, *J. Cell Biol.*, 2004, **166**, 877–887.
11 S. R. Peyton and A. J. Putnam, *J. Cell. Physiol.*, 2005, **204**, 198–209.
12 G. Y. Jiang, A. H. Huang, Y. F. Cai, M. Tanase and M. P. Sheetz, *Biophys. J.*, 2006, **90**, 1804–1809.
13 W. H. Guo, M. T. Frey, N. A. Burnham and Y. L. Wang, *Biophys. J.*, 2006, **90**, 2213.
14 D. E. Ingber, *Int. J. Dev. Biol.*, 2006, **50**, 255–266.
15 A. J. Engler, S. Sen, H. L. Sweeney and D. E. Discher, *Cell*, 2006, **126**, 677–689.
16 K. Ghosh, Z. Pan, E. Guan, S. Ge, Y. Liu, T. Nakamura, X. D. Ren, M. Rafailovich and R. A. F. Clark, *Biomaterials*, 2007, **28**, 671–679.
17 R. J. Pelham and Y. L. Wang, *Proc. Natl. Acad. Sci. U. S. A.*, 1997, **94**, 13661–13665.
18 T. Yeung, P. C. Georges, L. A. Flanagan, B. Marg, M. Ortiz, M. Funaki, N. Zahir, W. Y. Ming, V. Weaver and P. A. Janmey, *Cell Motil. Cytoskeleton*, 2005, **60**, 24–34.
19 N. Wang and D. E. Ingber, *Biophys. J.*, 1994, **66**, 2181–2189.
20 A. P. Balgude, X. Yu, A. Szymanski and R. V. Bellamkonda, *Biomaterials*, 2001, **22**, 1077–1084.
21 L. A. Flanagan, Yo-El. Ju, B. Marg, M. Osterfield and P. A. Janmey, *NeuroReport*, 2002, **13**, 2411–2415.
22 P. C. Georges, W. J. Miller, D. F. Meaney, E. S. Sawyer and P. A. Janmey, *Biophys. J.*, 2006, **90**, 3012–3018.
23 P. C. Dartsch and E. Betz, *Basic Res. Cardiol.*, 1989, **84**, 268–281.
24 C. Neidlinger-Wilke, E. S. Grood, J. H. C. Wang, R. A. Brand and L. Claes, *J. Orthop. Res.*, 2001, **19**, 286–293.
25 J. H.-C. Wang, *J. Theor. Biol.*, 2000, **202**, 33–41.
26 R. Kaunas, P. Nguyen, S. Usami and S. Chien, *Proc. Natl. Acad. Sci. U. S. A.*, 2005, **102**, 15895–15900.
27 C. M. Lo, H. B. Wang, M. Dembo and Y. L. Wang, *Biophys. J.*, 2000, **79**, 144–152.
28 J. Y. Wong, A. Velasco, P. Rajagopalan and Q. Pham, *Langmuir*, 2003, **19**, 1908–1913.
29 A. Engler, L. Bacakova, C. Newman, A. Hategan, M. Griffin and D. Discher, *Biophys. J.*, 2004, **86**, 617–628.
30 A. Saez, M. Ghibaudo, A. Buguin, P. Silberzan and B. Ladoux, *Proc. Natl. Acad. Sci. U. S. A.*, 2007, **104**, 8281–8286.
31 J. D. Murray and G. F. Oster, *J. Math. Biol.*, 1984, **19**, 265–279.
32 I. B. Bischofs and U. S. Schwarz, *Proc. Natl. Acad. Sci. U. S. A.*, 2003, **100**, 9274–9279.
33 I.. B. Bischofs, S. A. Safran and U. S. Schwarz, *Phys. Rev. E: Stat. Phys., Plasmas, Fluids, Relat. Interdiscip. Top.*, 2004, **69**, 021911.
34 P. Namy, J. Ohayon and P. Tracqui, *J. Theor. Biol.*, 2004, **227**, 103–120.
35 R. Bar-Ziv, T. Tlusty, E. Moses, S. A. Safran and A. Bershadsky, *Proc. Natl. Acad. Sci. U. S. A.*, 1999, **96**, 10140–10145.
36 I. L. Novak, B. M. Slepchenko, A. Mogilner and L. M. Loew, *Phys. Rev. Lett.*, 2004, **93**, 268109.
37 J. P. McGarry, B. P. Murphy and P. E. McHugh, *J. Mech. Phys. Solids*, 2005, **53**, 2597–2637.
38 S. H. Chen and H. J. Gao, *Proc. R. Soc. London, Ser. A*, 2006, **462**, 211–228.
39 A. Nicolas and S. A. Safran, *Biophys. J.*, 2006, **91**, 61–73.
40 D. Raz-Ben Aroush and H. D. Wagner, *Adv. Mater.*, 2006, **18**, 1537–1540.
41 D. Stamenović, *Mol. Cell Biomech.*, 2005, **2**, 69–76.
42 D. Stamenović, *Mol. Cell Biomech.*, 2005, **3**, 43–48.
43 V. S. Deshpande, R. M. McMeeking and A. G. Evans, *Proc. Natl. Acad. Sci. U. S. A.*, 2006, **103**, 14015–14020.
44 V. S. Deshpande, R. M. McMeeking and A. G. Evans, *Proc. R. Soc. London, Ser. A*, 2007, **463**, 787–815.
45 N. D. Gallant and A. J. García, *J. Biomech.*, 2007, **40**, 1301–1309.
46 M. E. Gracheva and H. G. Othmer, *Bull. Math. Biol.*, 2004, **66**, 167–193.
47 M. H. Zaman, R. D. Kamm, P. Matsudaira and D. A. Lauffenburger, *Biophys. J.*, 2005, **89**, 1389–1397.
48 H. J. Gao, W. D. Shi and L. B. Freund, *Proc. Natl. Acad. Sci. U. S. A.*, 2005, **102**, 9469–9474.
49 K. Larripa and A. Mogilner, *Physica A*, 2006, **372**, 113–123.
50 B. Geiger, A. Bershadsky, R. Pankov and K. M. Yamada, *Nat. Rev. Mol. Cell Biol.*, 2001, **2**, 793–805.
51 K. A. Beningo and Y. L. Wang, *Trends Cell Biol.*, 2002, **12**, 79–84.
52 D. Choquet, D. P. Felsenfeld and M. P. Sheetz, *Cell*, 1997, **88**, 39–48.
53 D. Riveline, E. Zamir, N. Q. Balaban, U. S. Schwarz, T. Ishizaki, S. Narumiya, Z. Kam, B. Geiger and A. D. Bershadsky, *J. Cell Biol.*, 2001, **153**, 1175–1186.
54 J. W. Cahn and J. E. Hilliard, *J. Chem. Phys.*, 1958, **28**, 258–267.
55 T. Bickel and R. Bruinsma, *arXiv.org*, 2003, cond-mat/0306116.
56 M. Dembo and Y. L. Wang, *Biophys. J.*, 1999, **76**, 2307–2316.
57 N. Q. Balaban, U. S. Schwarz, D. Riveline, P. Goichberg, G. Tzur, I. Sabanay, D. Mahalu, S. Safran, A. Bershadsky, L. Addadi and B. Geiger, *Nat. Cell Biol.*, 2001, **3**, 466–472.
58 J. L. Tan, J. Tien, D. M. Pirone, D. S. Gray, K. Bhadriraju and C. S. Chen, *Proc. Natl. Acad. Sci. U. S. A.*, 2003, **100**, 1484–1489.
59 O. du Roure, A. Saez, A. Buguin, R. H. Austin, P. Chavrier, P. Siberzan and B. Ladoux, *Proc. Natl. Acad. Sci. U. S. A.*, 2005, **102**, 2390–2395.
60 D. Stamenović and N. Wang, *J. Appl. Physiol.*, 2000, **89**, 2085–2090.
61 N. Wang, K. Naruse, D. Stamenović, J. J. Fredberg, S. M. Mijailovich, I. M. Toric-Norrelykke, T. Polte, R. Mannix and D. E. Ingber, *Proc. Natl. Acad. Sci. U. S. A.*, 2001, **98**, 7765–7770.
62 N. Wang, I. M. Tolic-Norrelykke, J. X. Chen, S. M. Mijailovich, J. P. Butler, J. J. Fredberg and D. Stamenović, *Am. J. Physiol.: Cell Physiol.*, 2002, **282**, C606–C616.
63 R. Bruinsma, *Biophys. J.*, 2005, **89**, 87–94.
64 A. Zemel, I. B. Bischofs and S. A. Safran, *Phys. Rev. Lett.*, 2006, **97**, 128103.
65 U. S. Schwarz, E. Erdmanm and I. B. Bischofs, *Biosystems*, 2006, **83**, 225–232.
66 K. M. Yamada and B. Geiger, *Curr. Opin. Cell Biol.*, 1997, **9**, 76–85.
67 T. Shemesh, B. Geiger, A. D. Bershadsky and M. M. Kozlov, *Proc. Natl. Acad. Sci. U. S. A.*, 2005, **102**, 12383–12388.
68 J. M. Deutch and F. E. Low, *J. Phys. Chem.*, 1992, **96**, 7097–7101.
69 L. Q. Chen and J. Shen, *Comput. Phys. Commun.*, 1998, **108**, 147–158.
70 V. B. Shenoy and L. B. Freund, *Proc. Natl. Acad. Sci. U. S. A.*, 2005, **102**, 3213–3218.
71 A. Besser and S. A. Safran, *Biophys. J.*, 2006, **90**, 3469–3484.
72 T. Erdmann and U. S. Schwarz, *Biophys. J.*, 2006, **91**, L60–L62.
73 M. Asfaw, B. Różycki, R. Lipowsky and T. R. Weikl, *Europhys. Lett.*, 2006, **76**, 703–709.
74 N. S. Gov, *Biophys. J.*, 2006, **91**, 2844–2847.

